Electronic Supplementary Information (ESI)

Cerium-Doping and Nitridation Effects on Nickel-based Metal Organic Framework for Alkaline Water Oxidation

Chikaodili E. Chukwuneke[1,4], Kenta Kawashima[1], Tran Phuoc Anh Nguyen[1], Gabriella Ruiz[1], Jing Lian Ng[2], Johnpaul Smith[1], Raul A. Marquez[1], Jay T. Bender[2], Xun Zhan[3], Wennie Wang[2,3,4], Delia J. Milliron[1,2,3], Michael J. Rose[1,4], C. Buddie Mullins[1,2,3,4,5,*]

[1.] *Department of Chemistry, The University of Texas at Austin, Austin, Texas 78712, United States*

[2.] *McKetta Department of Chemical Engineering, The University of Texas at Austin, Austin, Texas 78712, United States*

[3.] *Texas Materials Institute, The University of Texas at Austin, Texas 78712, United States*

[4.] *Allen J. Bard Center for Electrochemistry, The University of Texas at Austin, Austin, Texas 78712, United States*

[5.] *H2@UT, The University of Texas at Austin, Austin, Texas 78712, United States*

**Corresponding author.*

E-mail address: mullins@che.utexas.edu

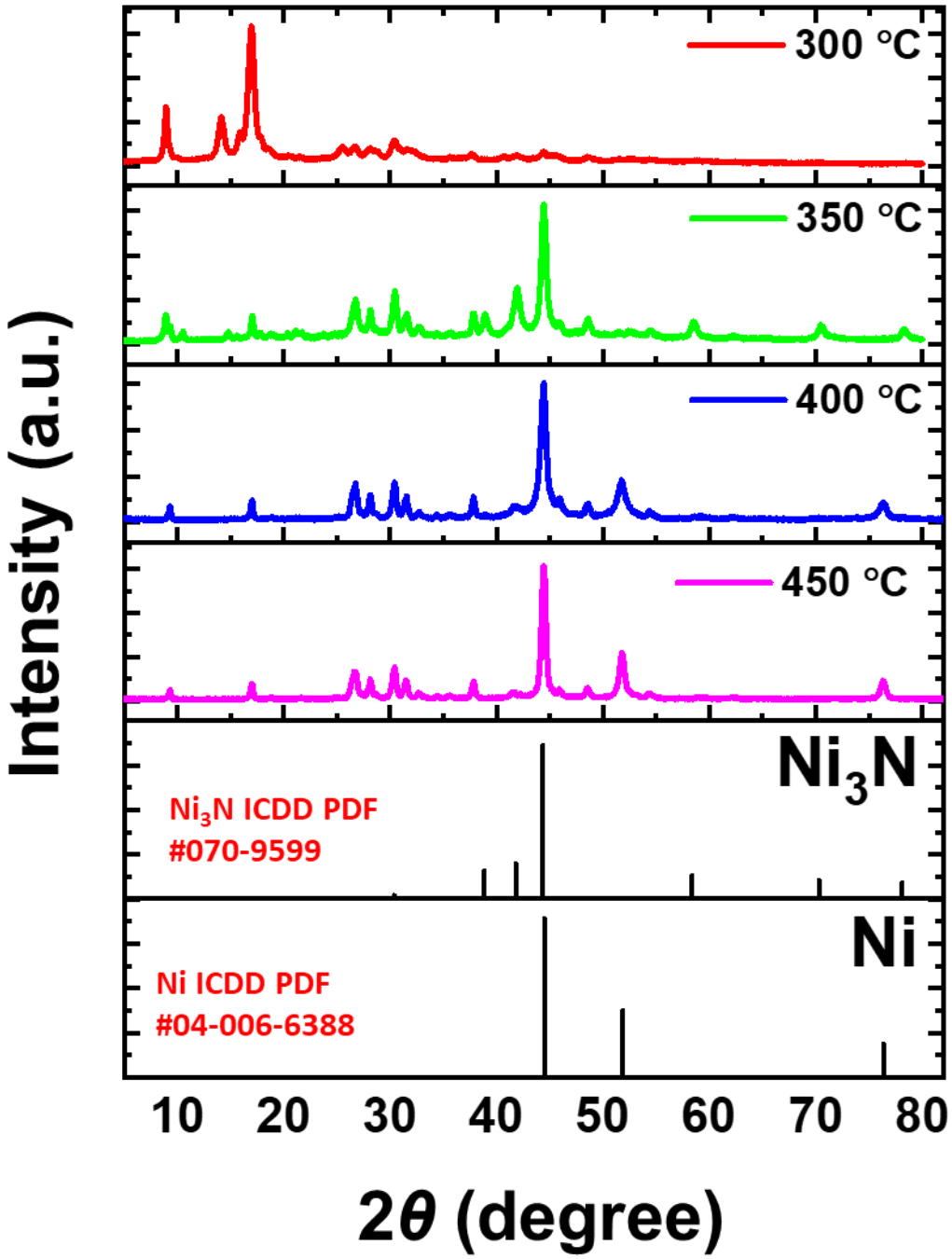

Figure S1. XRD patterns of the nitride phase optimization process.

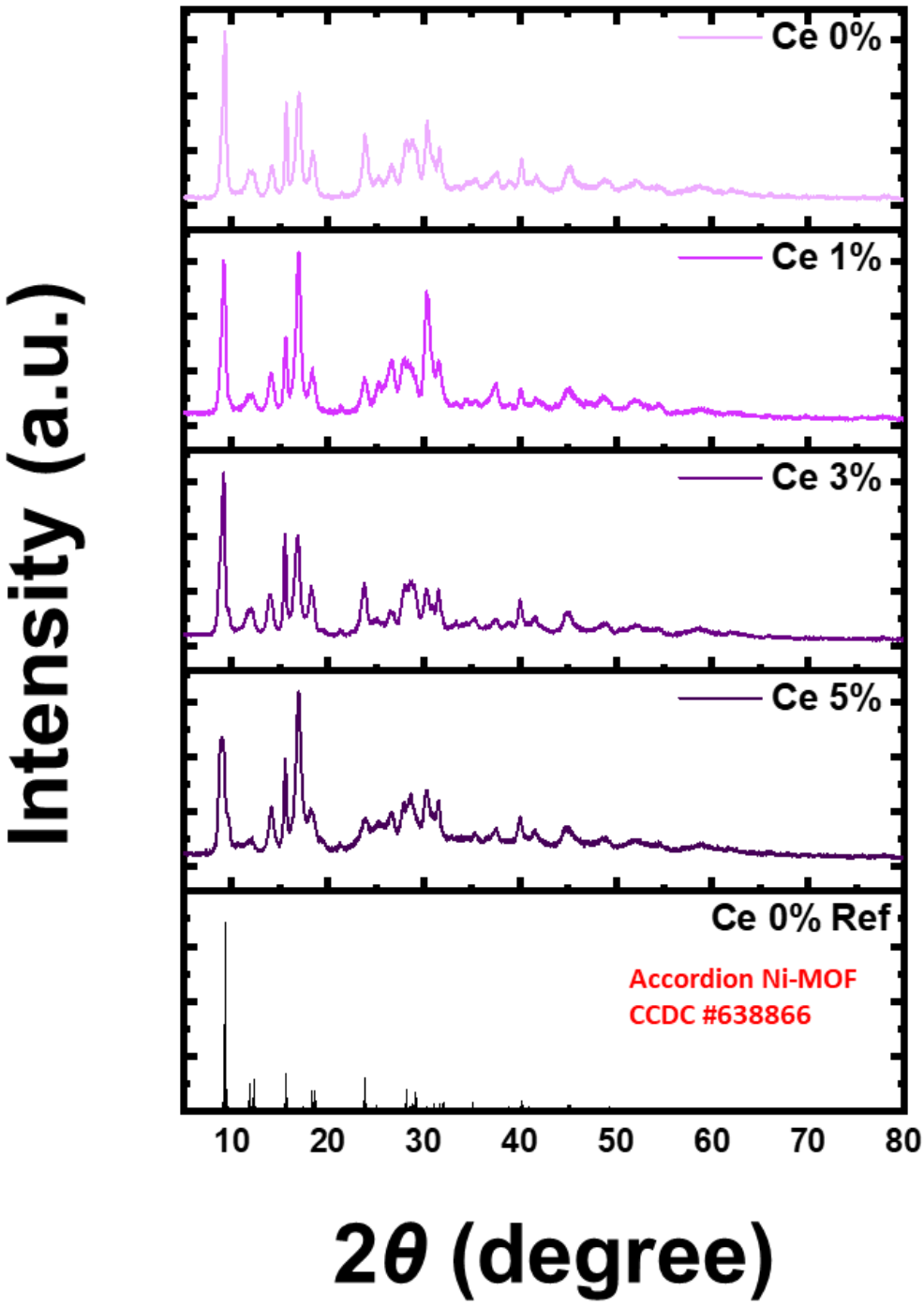

Figure S2. XRD patterns of pristine Ce_xNi_{1-x}-MOFs.

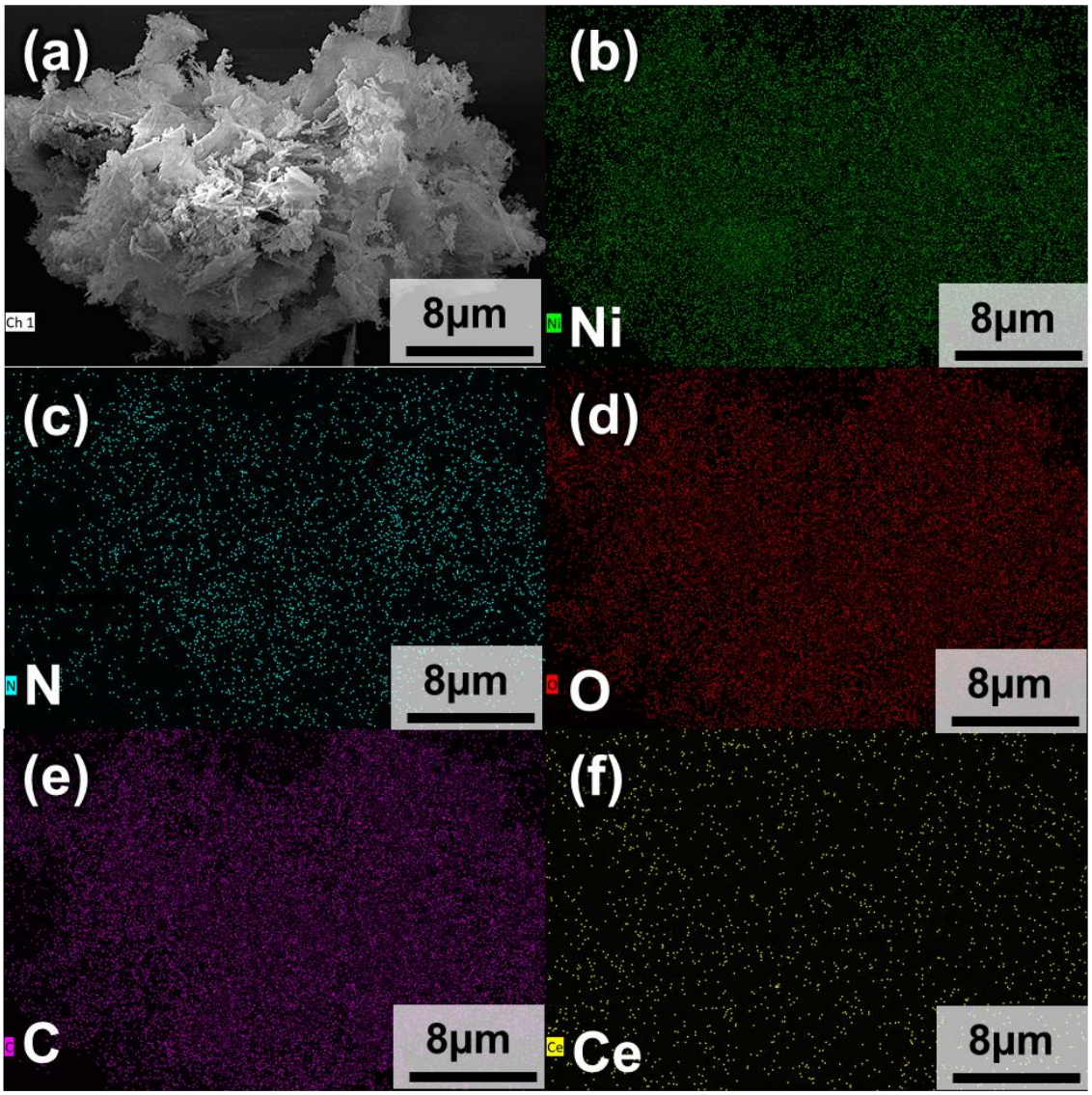

Figure S3. SEM and EDX elemental mapping images of Ce_0Ni_1-NMOF.

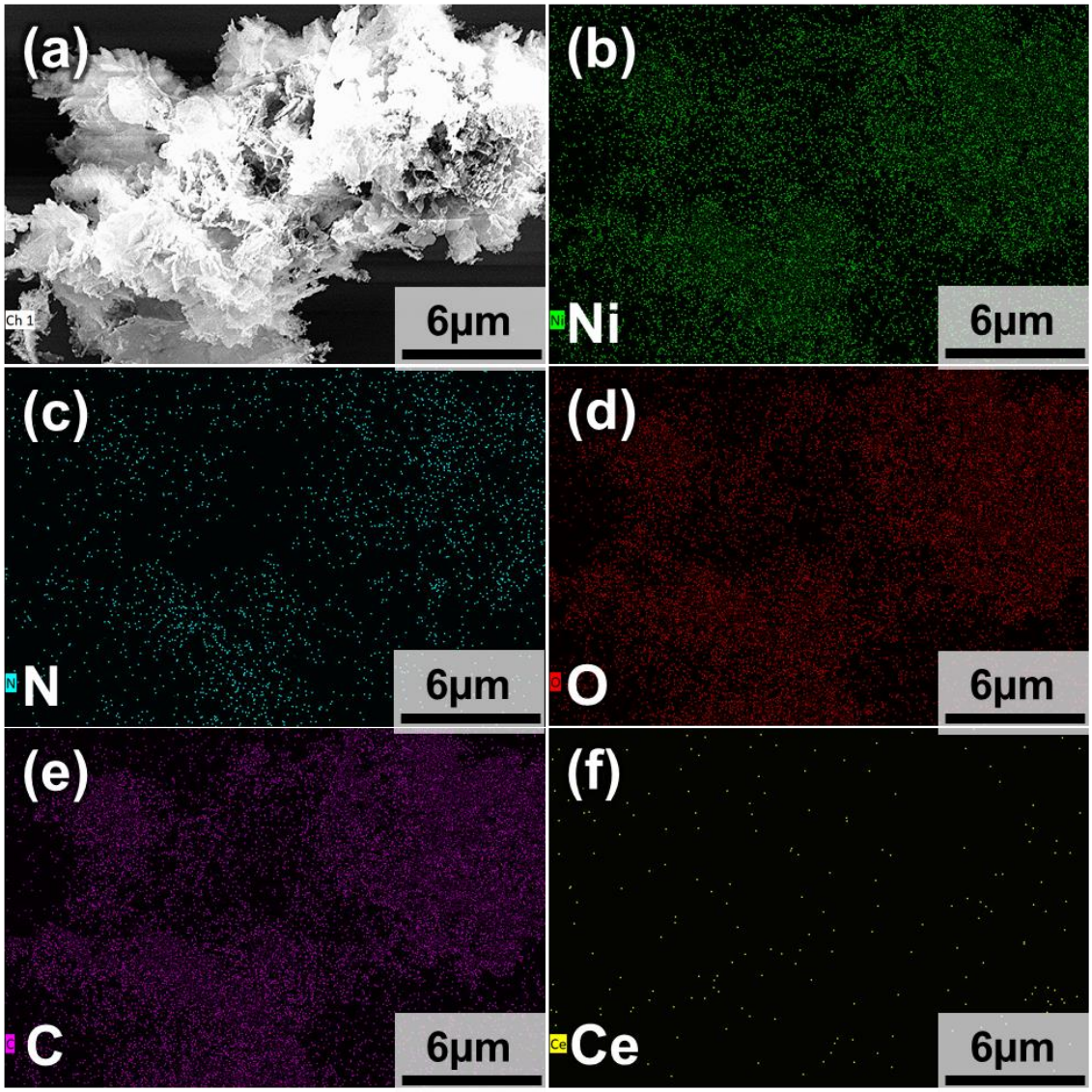

Figure S4. SEM and EDX elemental mapping images of $Ce_{0.01}Ni_{0.99}$-NMOF.

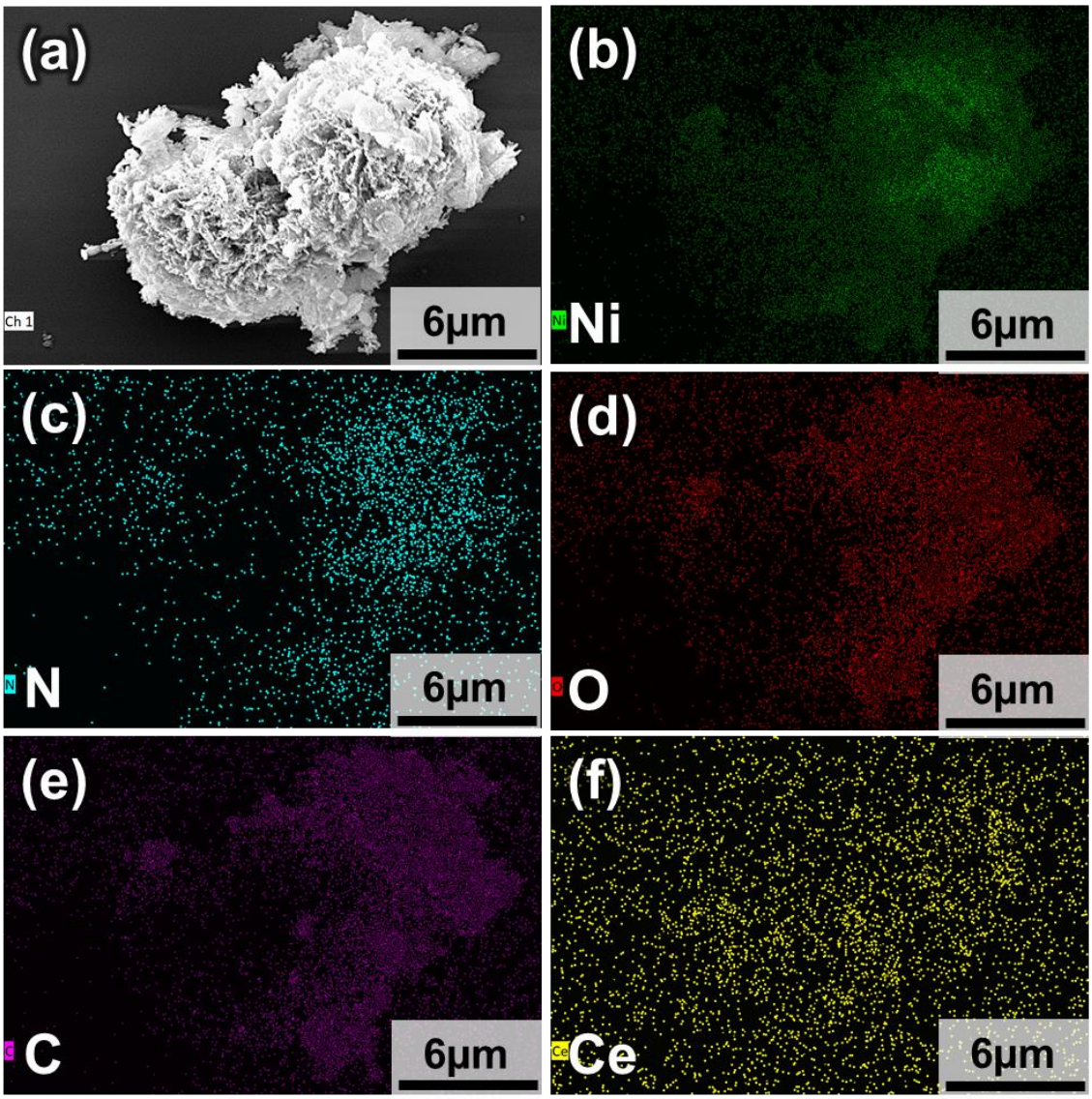

Figure S5. SEM and EDX elemental mapping images of $Ce_{0.05}Ni_{0.95}$-NMOF.

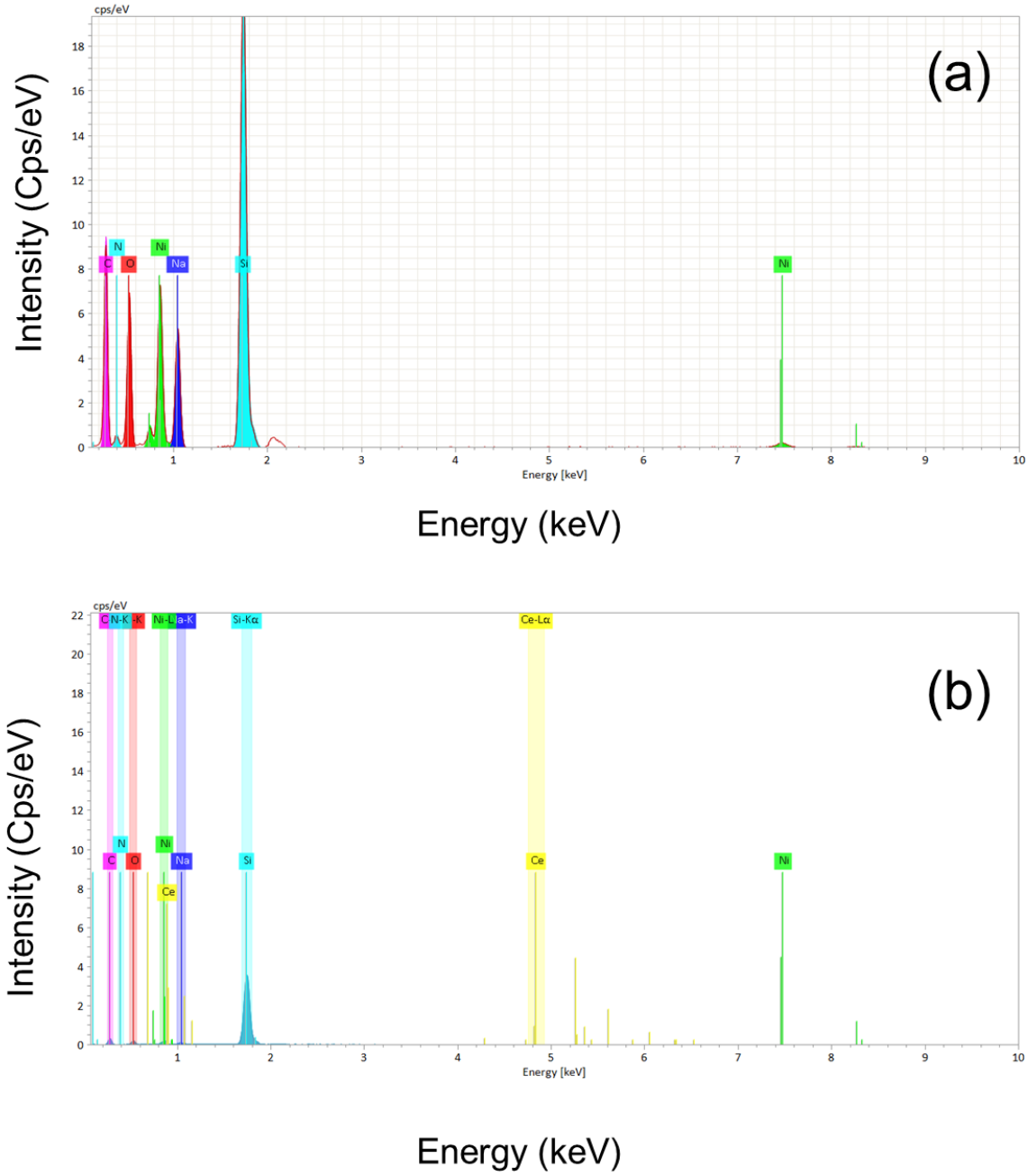

Figure S6. EDX spectra of (a) Ce_0Ni_1-NMOF and (b) $Ce_{0.01}Ni_{0.99}$-NMOF.

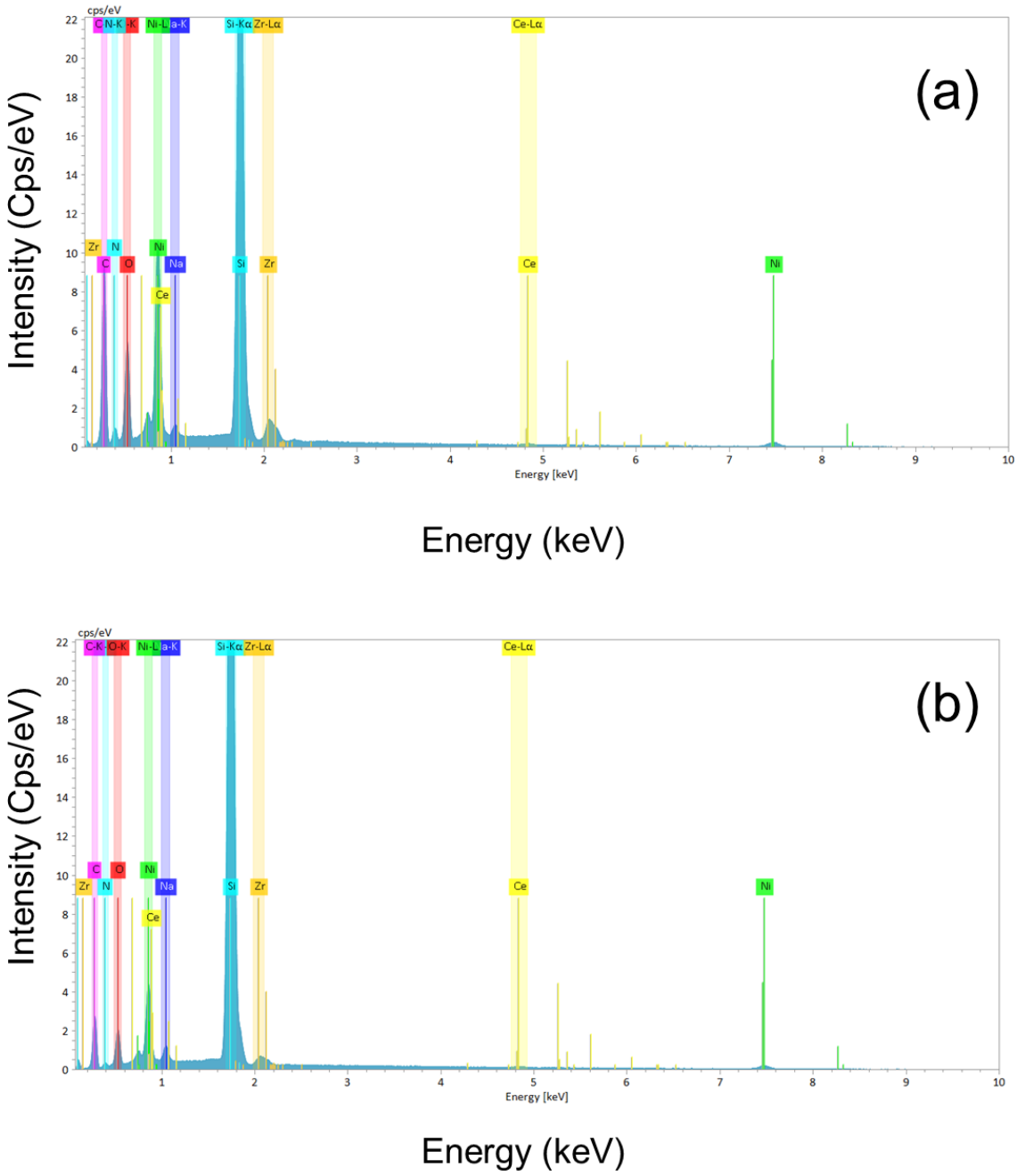

Figure S7. EDX spectra of (a) $Ce_{0.03}Ni_{0.97}$-NMOF and (b) $Ce_{0.05}Ni_{0.95}$-NMOF.

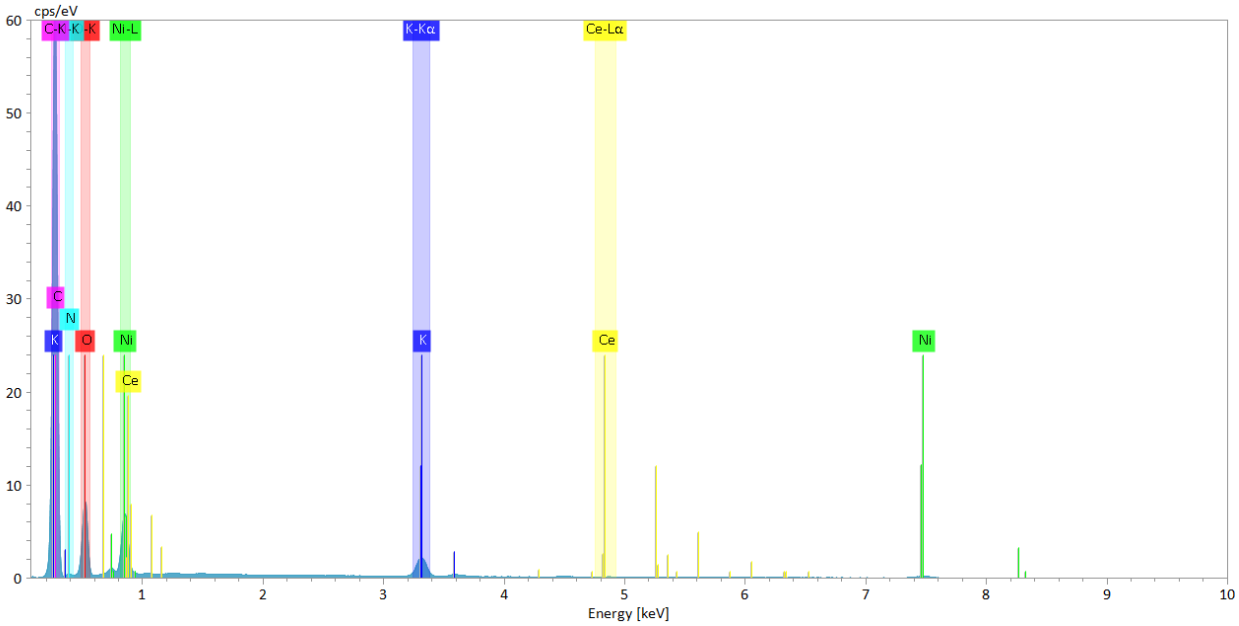

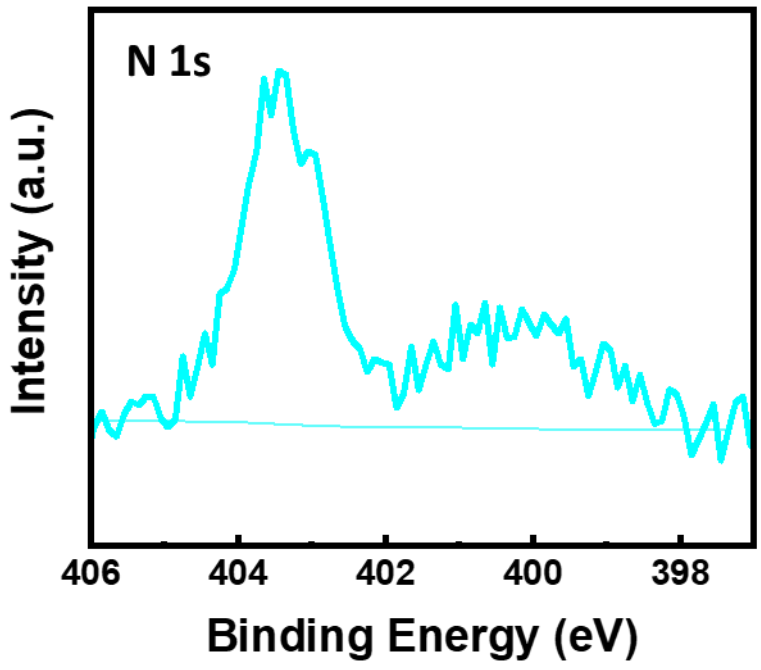

Figure S8. Post-OER (a) EDX (b) N 1s XPS spectra of $Ce_{0.03}Ni_{0.97}$-NMOF.

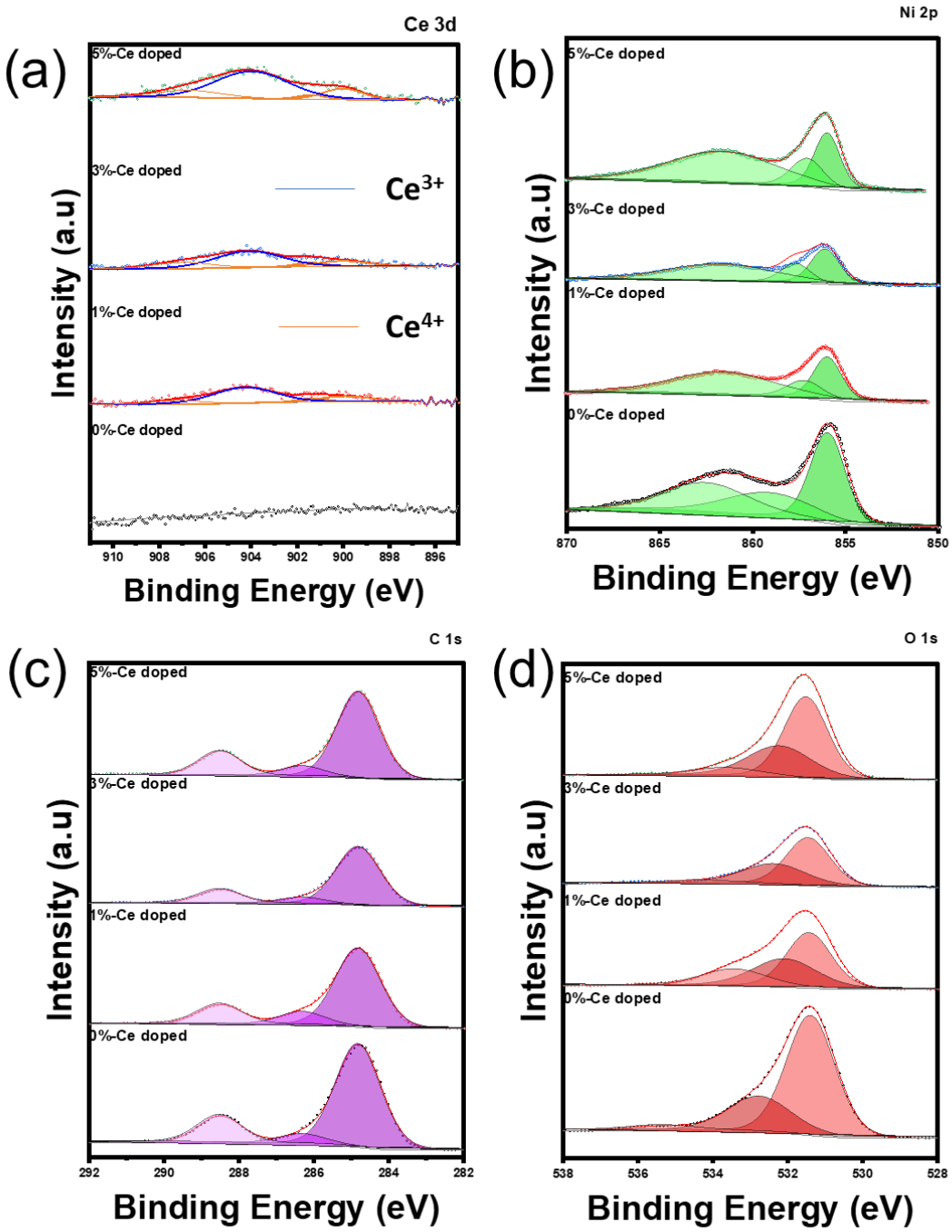

Figure S9. XPS spectra of Ce_xNi_{1-x}-MOF showing (a) Ce 3d, (b) Ni 2p, (c) C 1s, and (d) O 1s.

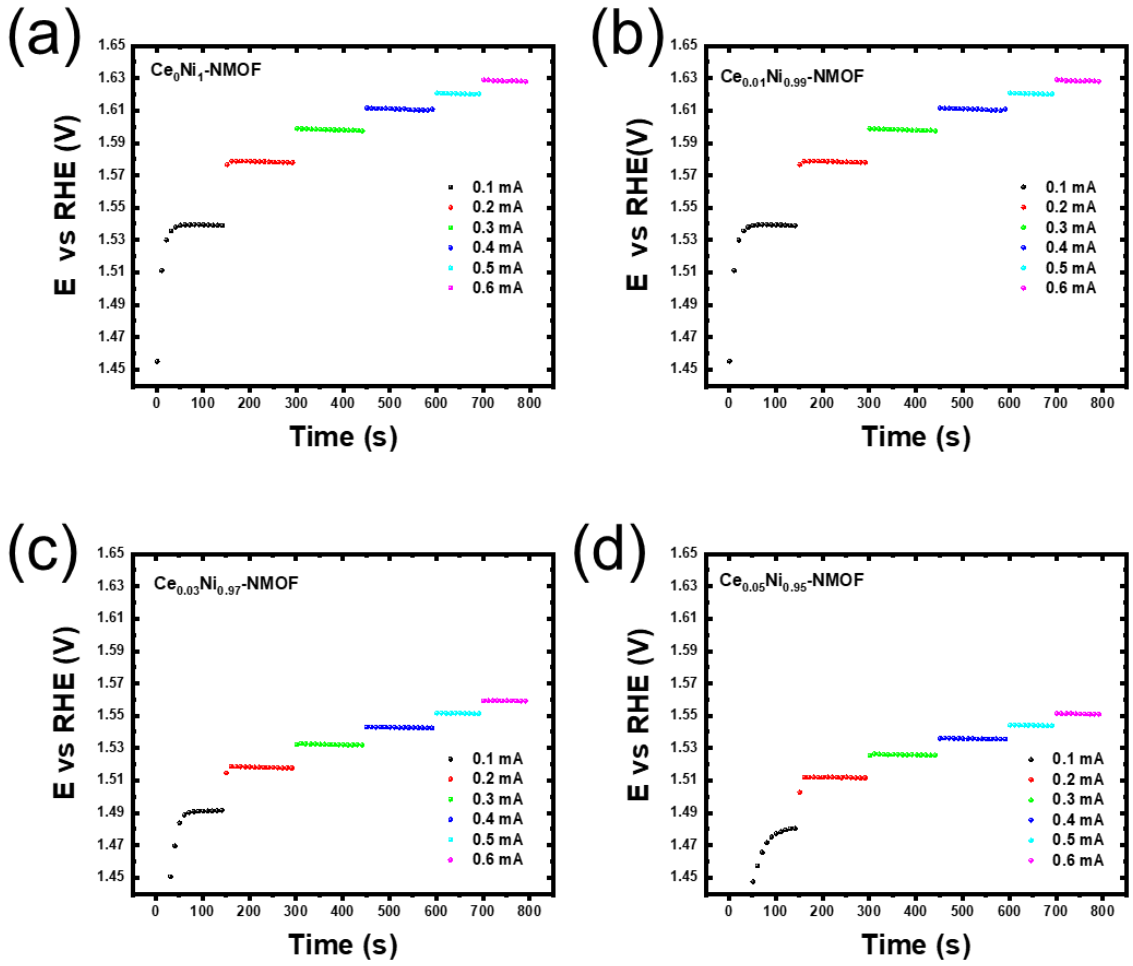

Figure S10. MUSCP plots for Ce_xNi_{1-x}-NMOF.

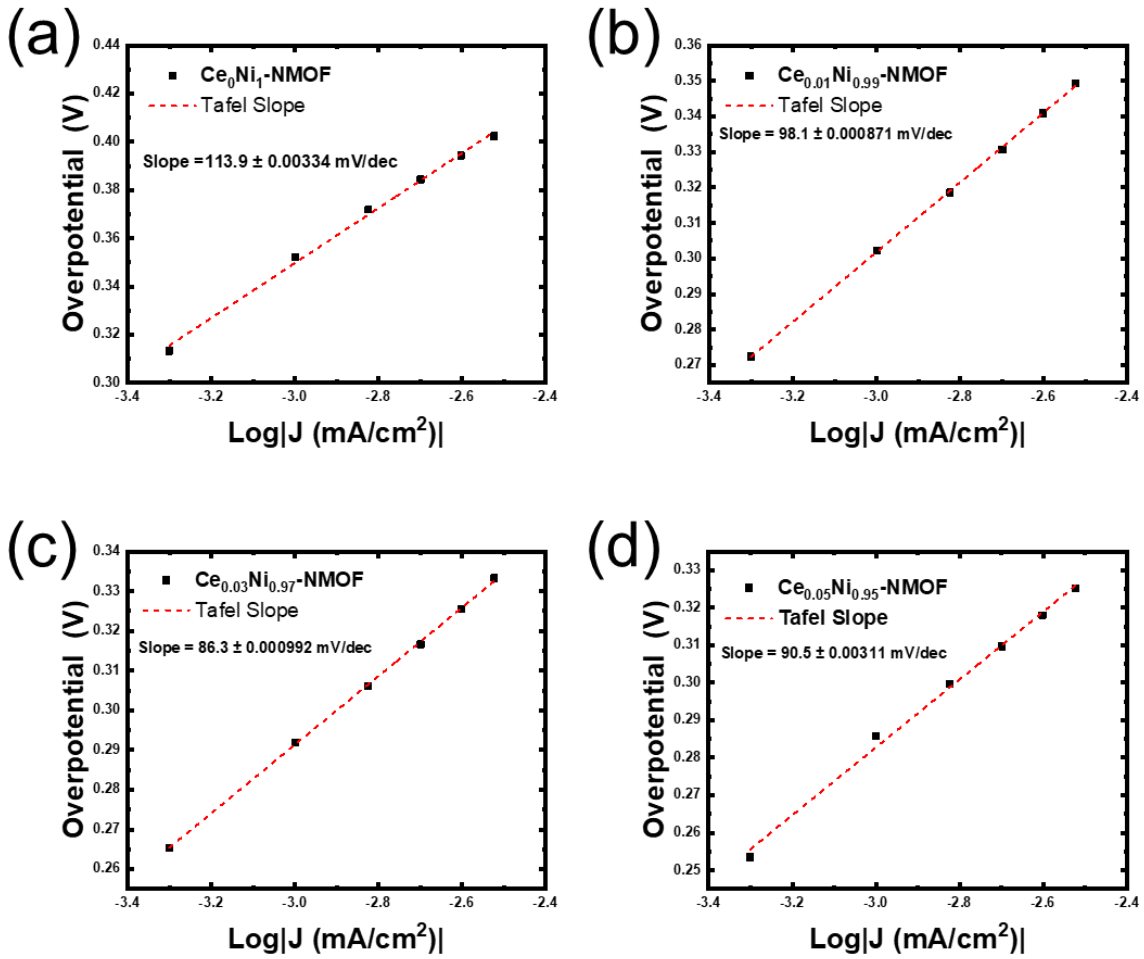

Figure S11. Tafel slopes from corresponding Ce_xNi_{1-x}-NMOF MUSCP plots.

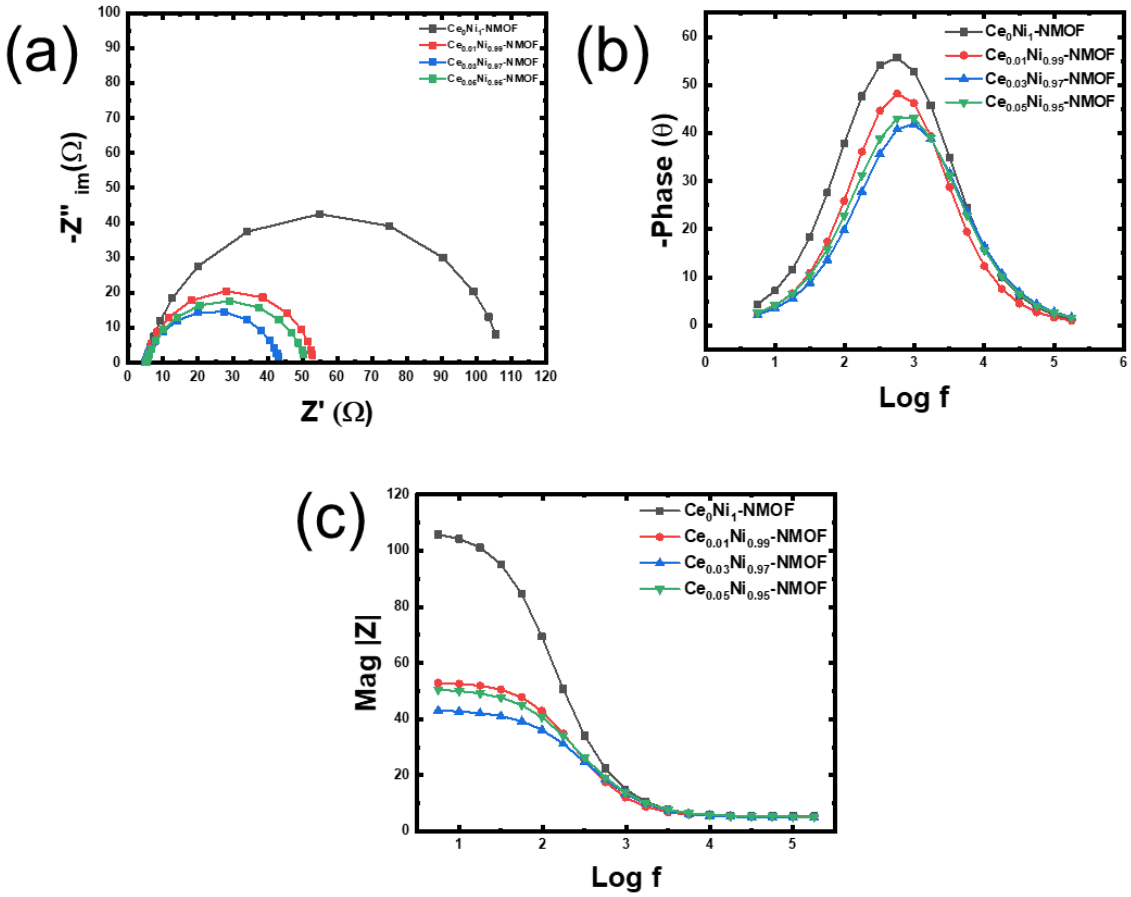

Figure S12. EIS results showing (a) Nyquist plots and (b and c) Bode plots for Ce_xNi_{1-x}-NMOF.

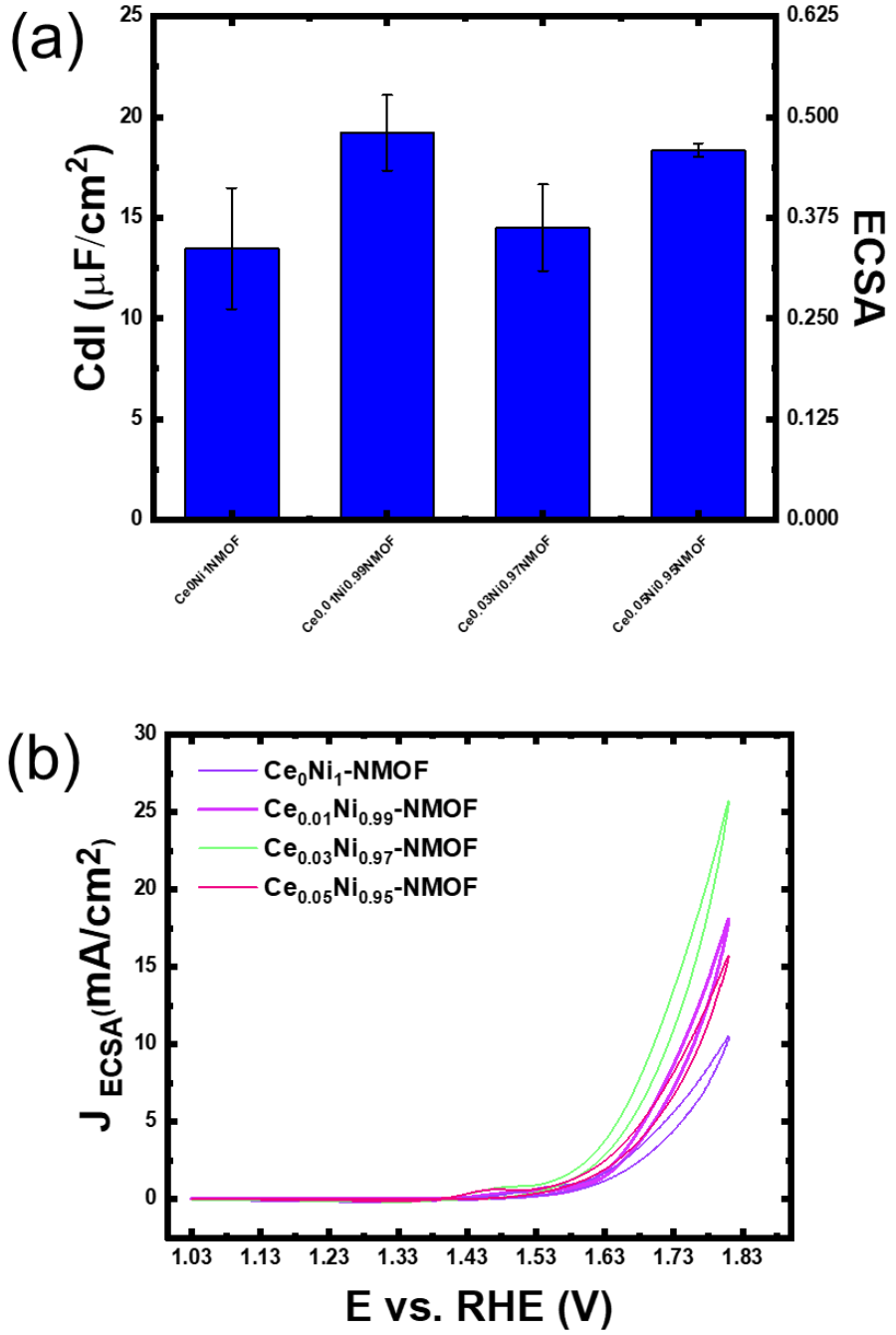

Figure S13. (a) Double-layer capacitance and ECSA values for Ce_xNi_{1-x}-NMOF. (b) ECSA normalized current for Ce_xNi_{1-x}-NMOF polarization curves.

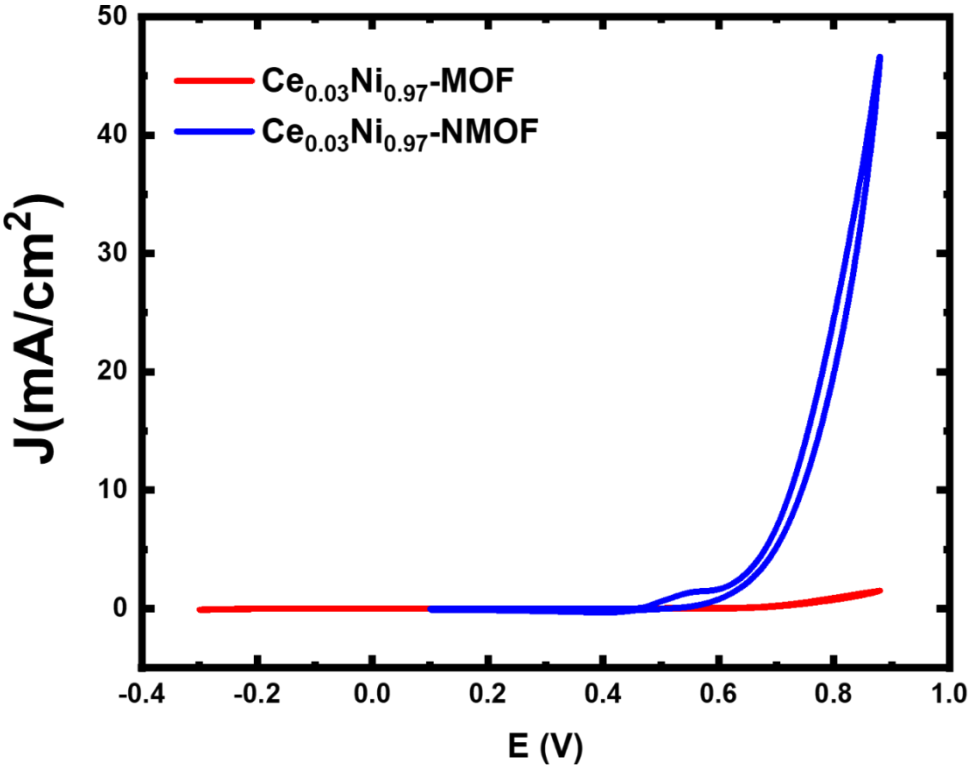

Figure S14. CV curves showing the effect of nitridation.

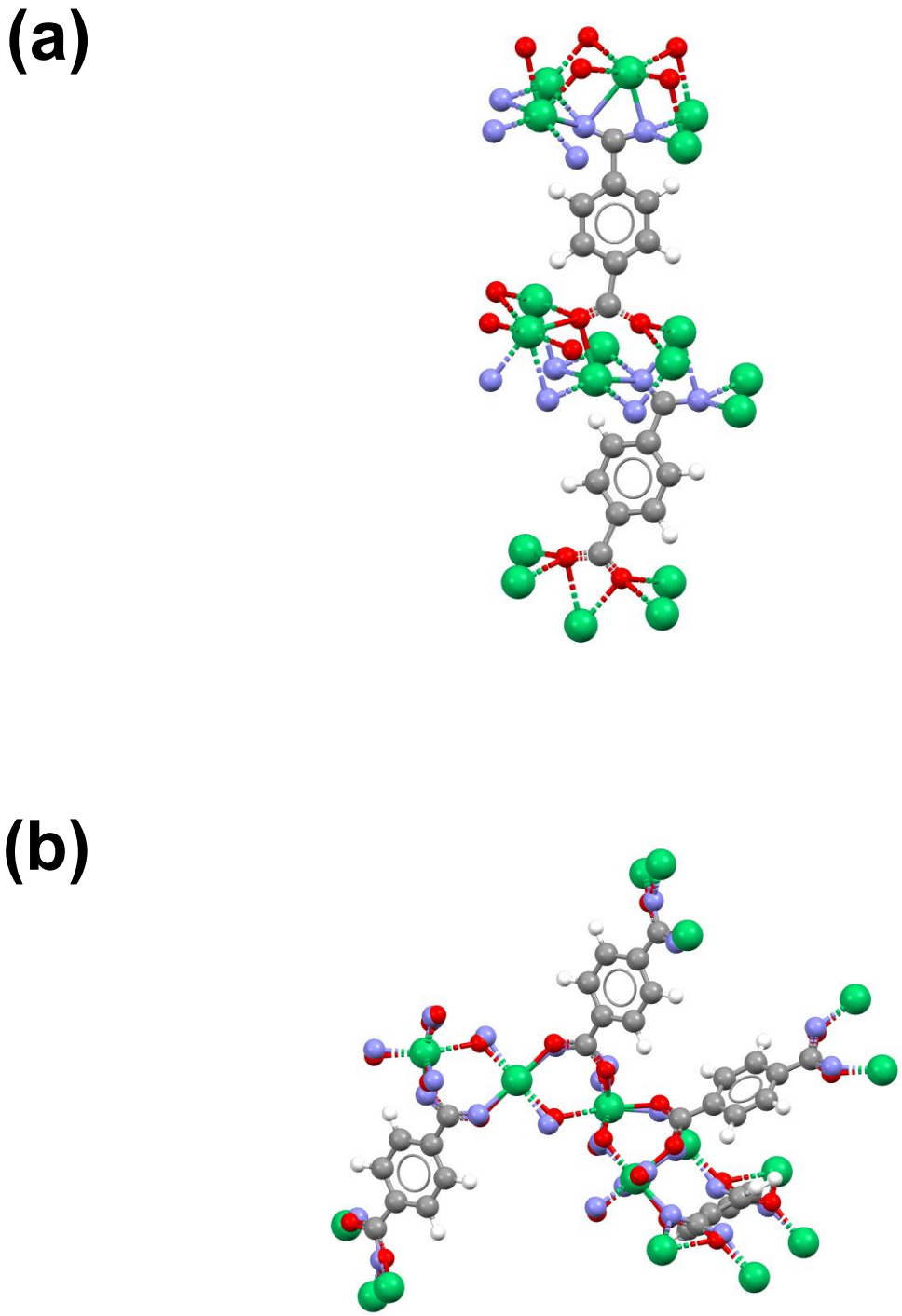

Figure S15. Micro-ED results of (a) Ce_0Ni_1-NMOF and (b) $Ce_{0.03}Ni_{0.97}$-NMOF.

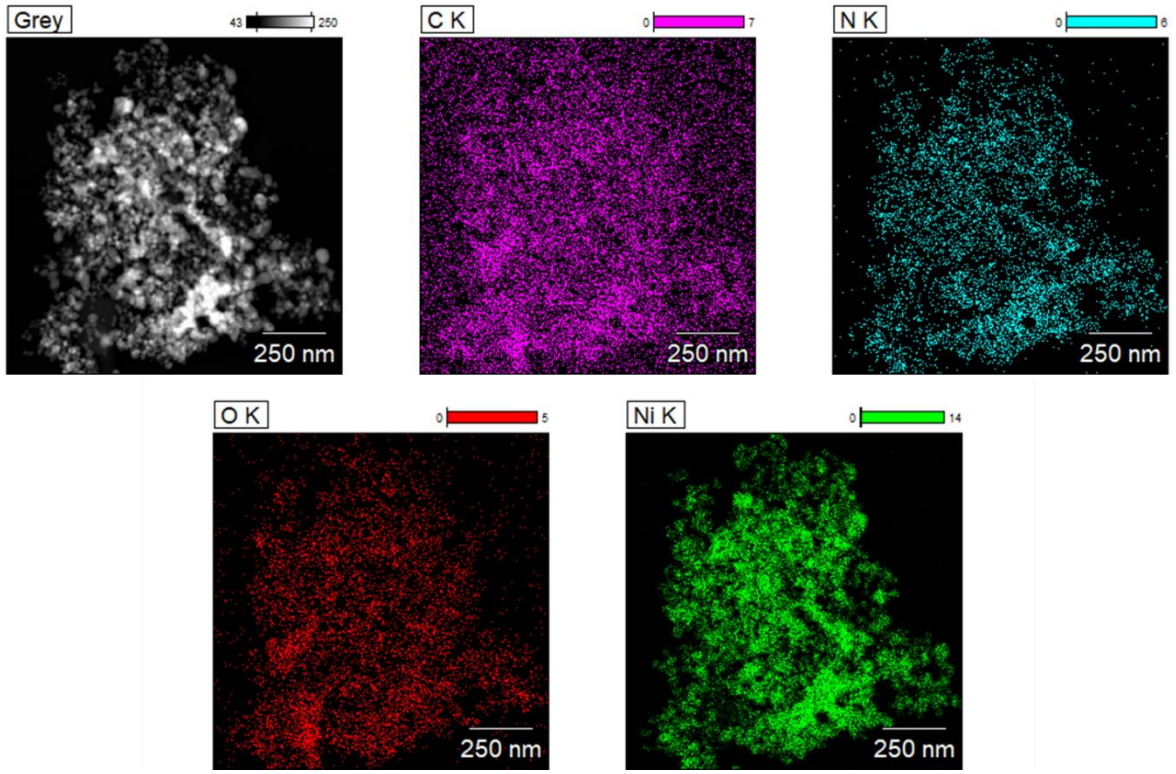

Figure S16. TEM and EDX elemental mapping images of Ce_0Ni_1-NMOF.

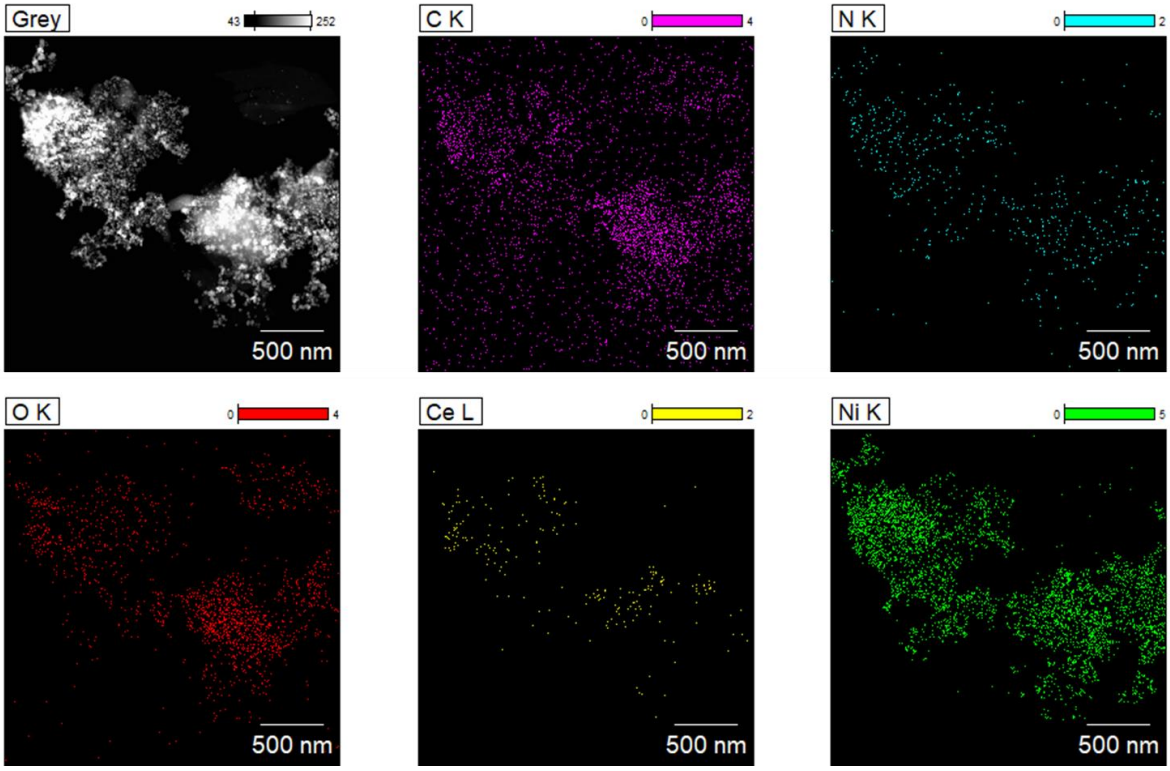

Figure S17. TEM and EDX elemental mapping images of $Ce_{0.03}Ni_{0.97}$-NMOF.

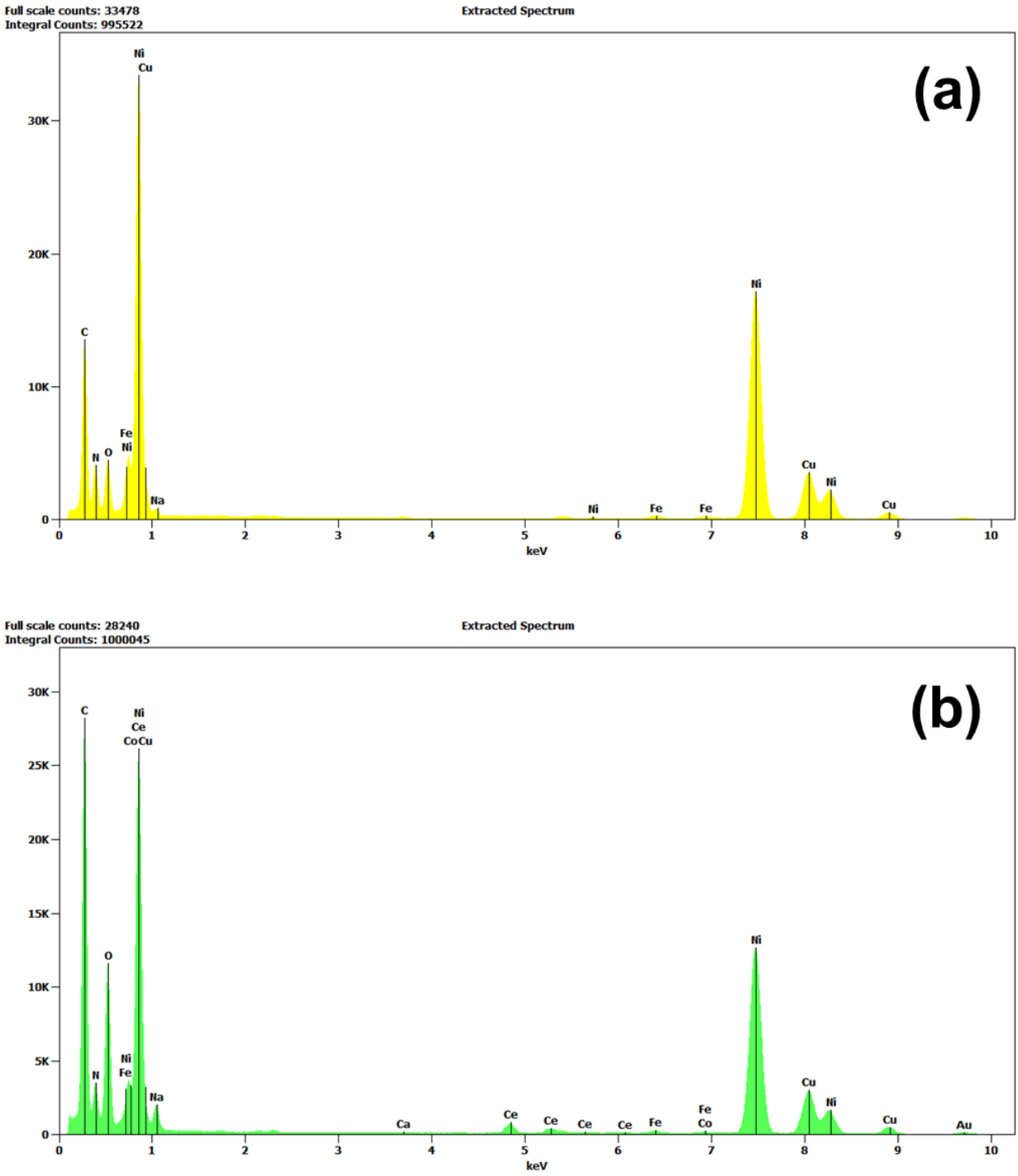

Figure S18. TEM-EDX spectra of (a) Ce_0Ni_1-NMOF and (b) $Ce_{0.03}Ni_{0.97}$-NMOF.

Table S1. ICP-MS determination of metallic distribution. *BDL: below detection limit

Elements		
Substance	Ni %	Ce %
Ce_0Ni_1-NMOF	99.9918	8.24E-05
$Ce_{0.01}Ni_{0.99}$-NMOF	97.5663	2.4337
$Ce_{0.03}Ni_{0.97}$-NMOF	91.3843	8.6157
$Ce_{0.05}Ni_{0.95}$-NMOF	87.6709	12.3291
Pristine KOH	NA	BDL
Post-OER KOH	NA	BDL

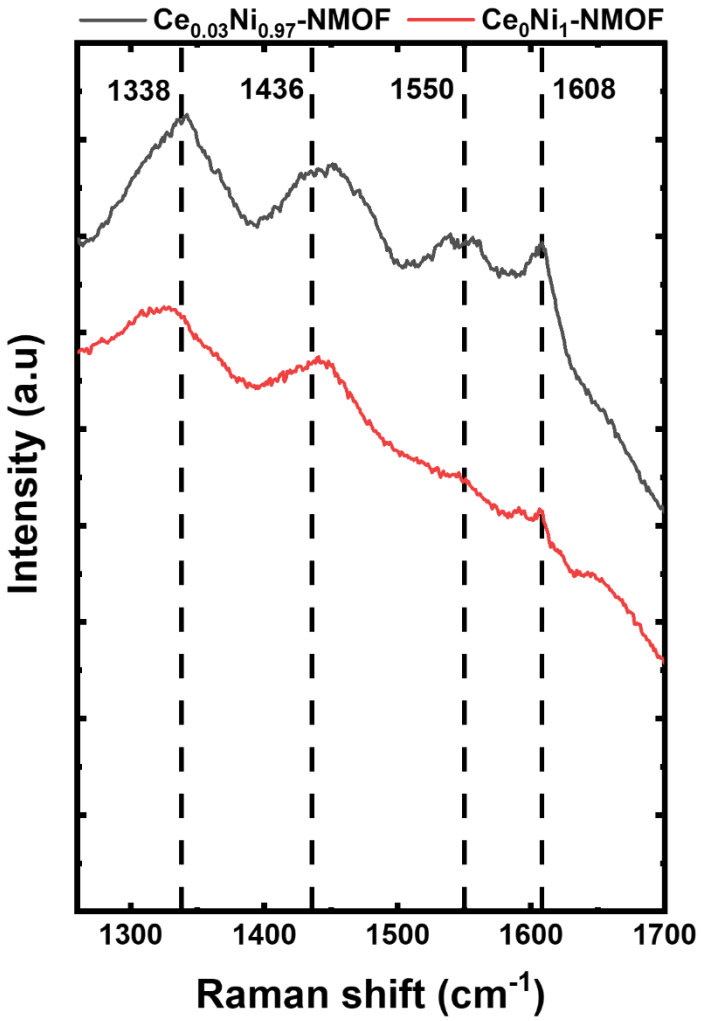

Figure S19. Post-OER *ex-situ* Raman spectra of Ce_0Ni_1-NMOF and $Ce_{0.03}Ni_{0.97}$-NMOF.

Table S2. Crystal data and refinement parameters

	Ce_0Ni_1-NMOF	$Ce_{0.03}Ni_{0.97}$-NMOF
Chemical Formula	$C_8H_4Ni_2O_4$	$C_{17}H_9Ni_3O_7$
FW	281.50	501.33
Crystal system, space group	Triclinic, P1	Triclinic, P-1
Temperature (K)	100	100
a,b,c (Å)	3.400(3), 5.200(4), 18.300(3)	8.600(3), 8.900(4), 10.600(3)
α, β, γ,	90.10(3), 90.20(3), 90.70(3),	112.50(3), 97.90(3), 94.90(3),
Volume ($Å^3$)	323.5(5)	734.0(5)
ρ (g/cm^3)	2.623	1.998
Z	4	4
Diffractometer	Thermo Fisher Glacios	Thermo Fisher Glacios
Accelerating voltage (kV)	200	200
Wavelength (Å)	0.025	0.025
Rotation rate (°/s)	1	1
# of crystals used	1	1
Resolution (Å)	0.65	0.70
Completeness (%)	63.3	63.1
R_σ	0.0894	0.1248
R_{int}	--	0.0784
R_1, wR_2, S [GooF]	0.3699, 0.6916	0.2121, 0.5022
Tot. No. of Reflections	3017	5675
No. of Independent Reflections	3017	2901

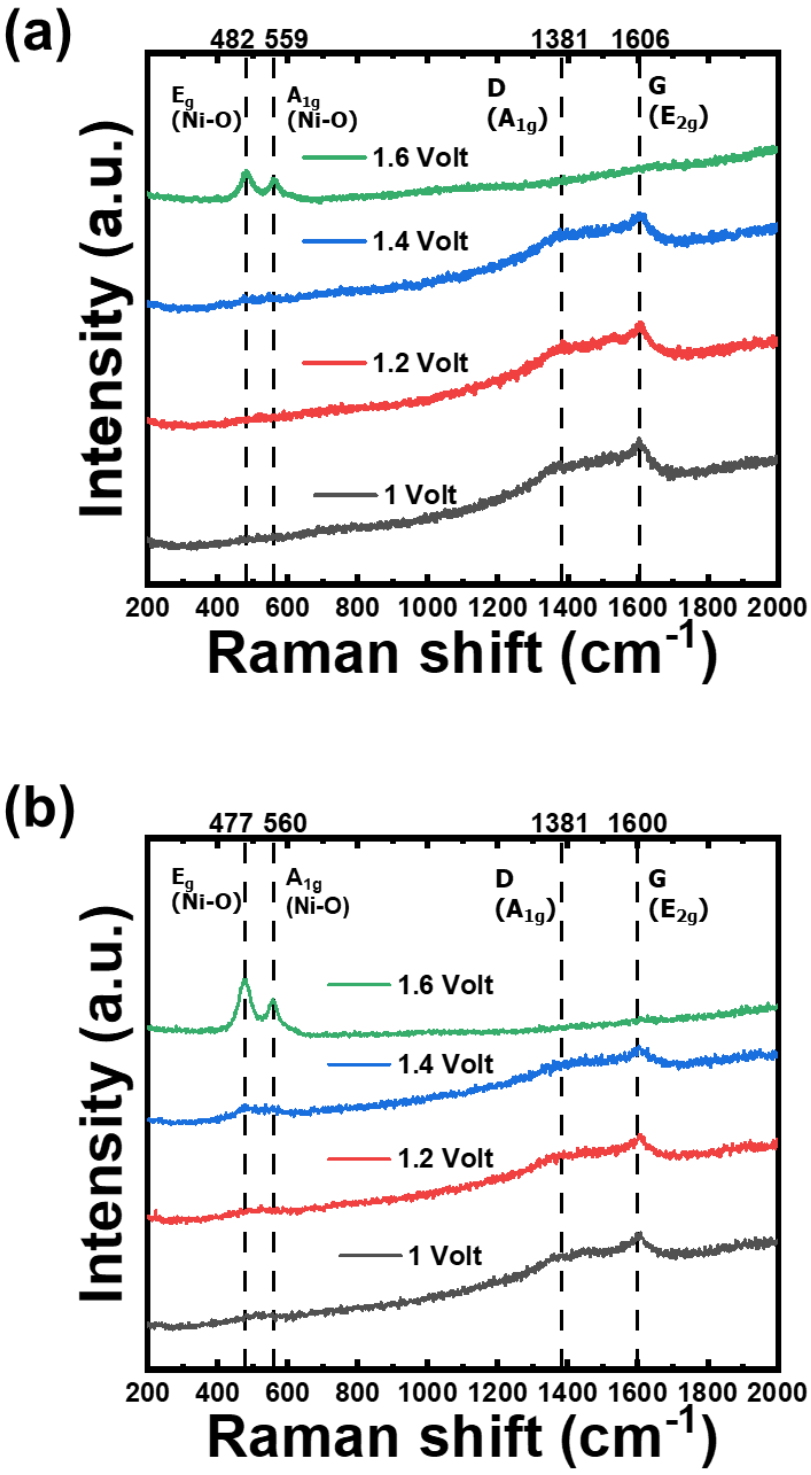

Figure S20. *In-situ* Raman measurements using a 514 nm laser at various potentials showing (a) NiOOH and graphitic carbon bands in Ce_0Ni_1-NMOF and (b) NiOOH and graphitic carbon bands in $Ce_{0.03}Ni_{0.97}$-NMOF.

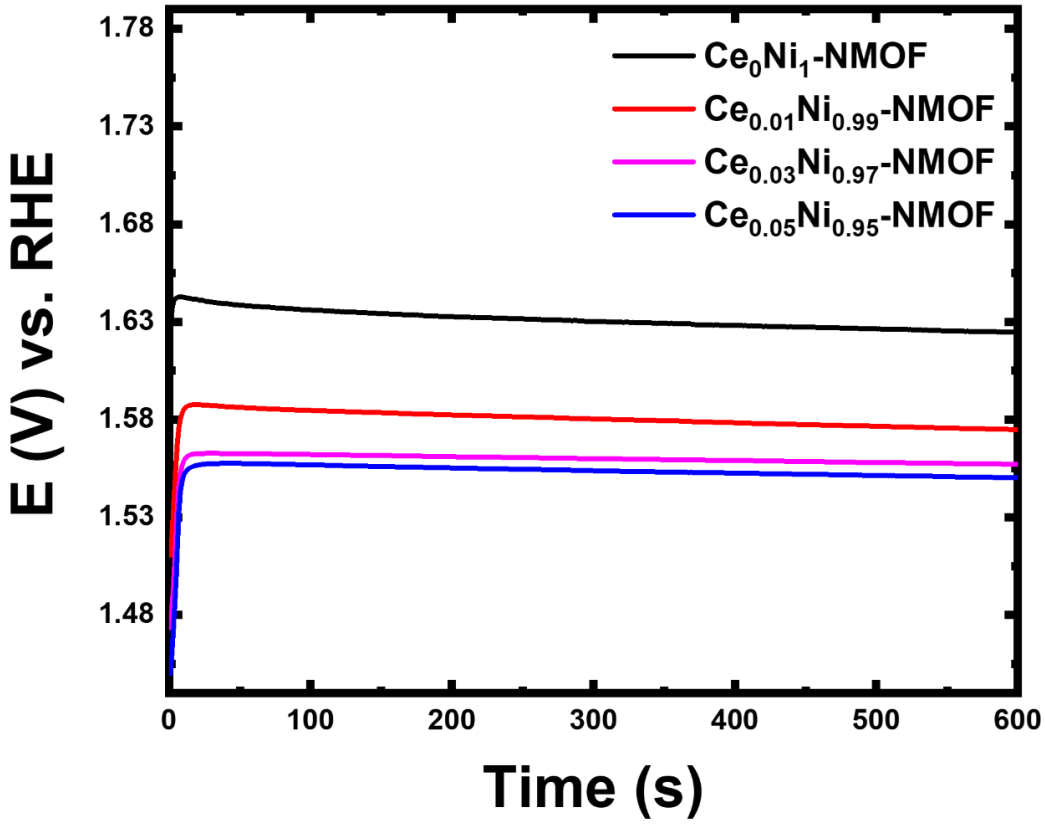

Figure S21. Chronopotentiometry of Ce_xNi_{1-x}-NMOF.

Supporting Note for Figure S21

Chronopotentiometry was conducted for 10 minutes to completely oxidize the precatalyst, creating a stable surface. This ensured that the current observed in the OER region is solely from OER currents and not a convoluting response from surface oxidation.

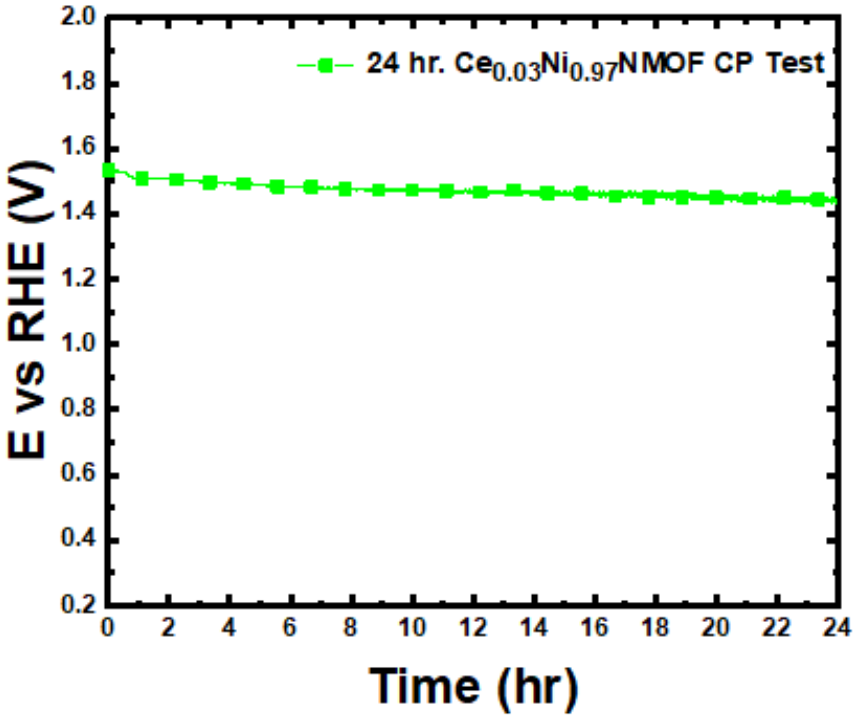

Figure S22. 24 h CP test for $Ce_{0.03}Ni_{0.97}$NMOF.

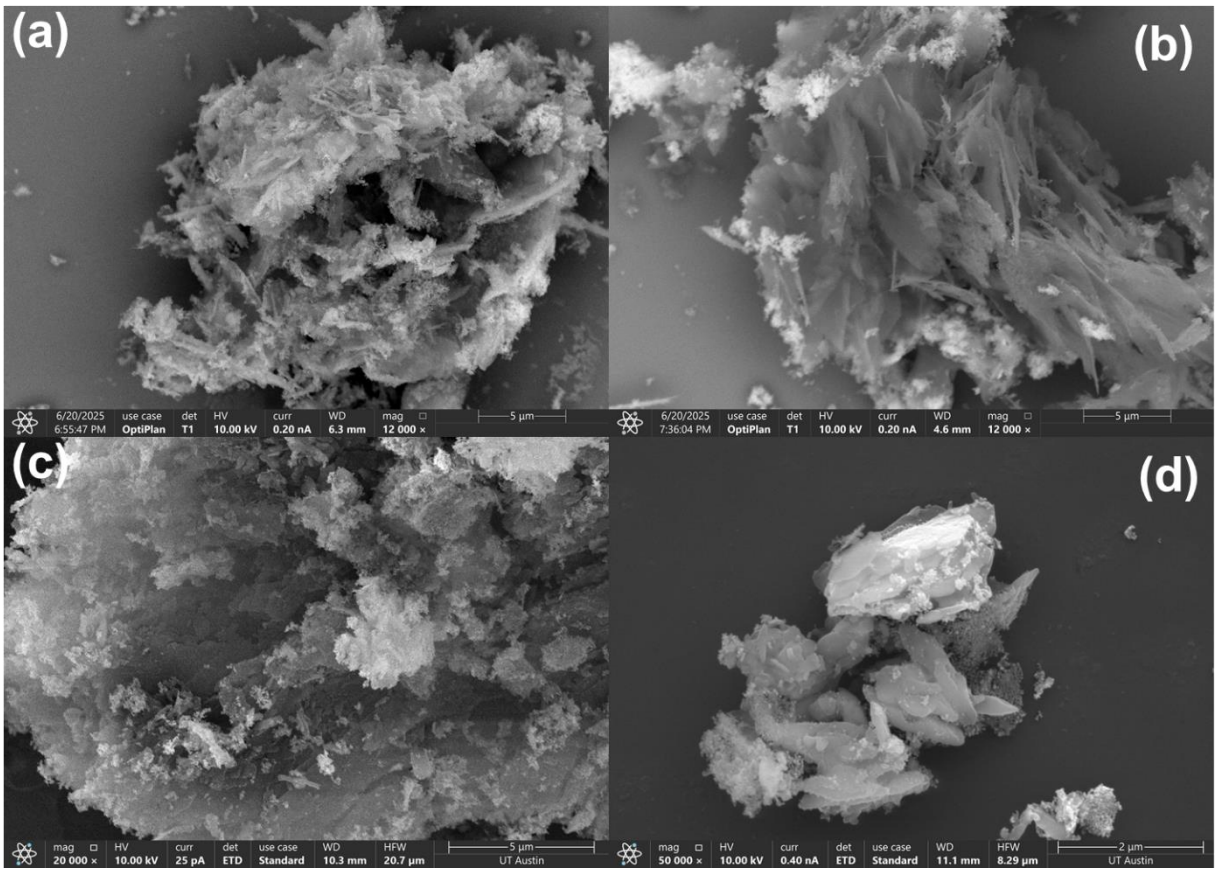

Figure S23. Scanning electron microscope images of (a) Ce_0Ni_1-NMOF, (b) $Ce_{0.01}Ni_{0.99}$-NMOF, (c) $Ce_{0.03}Ni_{0.97}$-NMOF, and (d) $Ce_{0.05}Ni_{0.95}$-NMOF.